



A Double Multi-Relaxation-Time Lattice Boltzmann Method for Simulation of Magneto Hydrodynamics Natural Convection of Nanofluid in a Square Cavity

A. R. Rahmati[†] and A. Najjarnezami

Department of Mechanical Engineering, Faculty of Engineering, University of Kashan, Kashan, Iran

[†]Corresponding Author Email: ar_rahmati@kashanu.ac.ir

(Received October 5, 2014; accepted April 20, 2015)

ABSTRACT

In this work, for the first time, a double multi-relaxation-time lattice Boltzmann method (2-MRT-LBM) is proposed to simulate MHD natural convection of nanofluid in a two-dimensional square cavity. The cavity is filled with TiO₂-water nanofluid and is get under a uniform magnetic field at different angles ϕ with respect to horizontal plane. The proposed numerical scheme is solved the flow field and the temperature field using MRT-D2Q9 and MRT-D2Q5 lattice model, respectively. So, the main objective of this work is to show the effectiveness of this model to predict the effects of pertinent parameters such as the Rayleigh number ($10^3 < Ra < 10^7$), the solid volume fraction ($0 \% < \phi < 5 \%$), the Hartmann number ($0 < Ha < 60$) and the magnetic field angle ($0 < \phi < 90$) on the flow field and temperature field and the heat transfer performance of the cavity. The obtained results indicate that the proposed method is a powerful approach to simulate the MHD natural convection of nanofluids in a square cavity. Also the numerical results show that for $Ra = 10^5$ and for the range of Hartmann number of this study, the heat transfer and fluid flow depend strongly upon the direction of magnetic field. Furthermore, the magnetic field influence on the effect of nanoparticles on the heat transfer enhancement is not significant.

Keywords: Magnetic field; Cavity; Natural convection; 2-MRT-LBM.

NOMENCLATURE

B	magnetic field strength	u, v	velocity components in x, y direction
c	magnitude of lattice streaming vectors	x, y	cartesian coordinates
c_i	lattice streaming vector in i direction		
C_p	specific heat	α	thermal diffusivity
F	external force	β	volume expansion coefficient
f_i	density distribution function	Δt	time step
f_i^{eq}	equilibrium density distribution function	Δx	lattice spacing
g	gravitational acceleration	μ	dynamic viscosity of fluid
g_i	temperature distribution function	Ω	collision operator
g_i^{eq}	equilibrium temperature distribution function	ϕ	solid volume fraction
Ha	Hartmann number	ϕ	magnetic field angle
k	thermal conductivity	σ	electrical conductivity
L	length of the cavity	ρ	density of fluid
n	lattice number	τ	relaxation time
M	transformation matrix	ω_i	weighted factor in i direction
m	moment	ν	kinematic viscosity
Ma	Mach number	Subscripts and Superscripts	
Nu	local Nusselt number	avg	average
Nu _{avg}	average Nusselt number	c	cold
p	pressure	eq	equilibrium
Pr	Prandtl number	f	fluid (pure water)
Ra	Rayleigh number	h	hot
T	temperature	i	lattice streaming vector direction
t	time	nf	nanofluid
		s	nanoparticle

1. INTRODUCTION

The problem of natural convection of electrically conducting fluids in the presence of magnetic field is one of the major interesting research subjects due to its widely engineering applications. For example, the effect of convection plays an important role in growing crystal from the melt because it can account for both heat and mass transfers in the liquid phase. These unavoidable hydrodynamic movements in crystal growth can be decreased with the help of a magnetic field (Vives and Perry, 1987; Utech and Flemmings, 1996).

The study of magnetic field has important applications in medicine, physics and engineering. Many industrial types of equipment, such as MHD generators, pumps, bearings and boundary layer control, are influenced by the interaction between the electrically conducting fluid and magnetic field. The behavior of the flow strongly depends on orientation and intensity of the applied magnetic field. The exerted magnetic field manipulates the suspended particles and rearranges their concentration in the fluid which strongly changes heat transfer characteristics of the flow. For this reason, many researchers have considered the magnetic field effects on the fluid flow field in different geometries (Aminossadati *et al.*, 2011; Mahmoudi *et al.*, 2012; and Rashidi *et al.*, 2013).

The MHD natural convection has been studied by many researchers using experimental, analytical and numerical methods. Okada and Ozoe (1992) carried out the experiments using molten gallium with Prandtl number of 0.024 in a cubical cavity heated from one side wall and cooled from the opposite wall with all other walls are insulated in the presence of different magnetic field direction, and found that the external magnetic field in the vertical direction was more effective than the magnetic field applied parallel to the heated vertical wall. Garandet *et al.* (1992) presented an analytical solution to model the effect of a transverse magnetic field on natural convection in a two dimensional cavity. Rudraiah *et al.* (1995) numerically studied the natural convection of an electrically conducting fluid in a rectangular cavity in the presence of a magnetic field. They have concluded that the average Nusselt number decreases with an increase in the Hartmann number and the Nusselt number approaches one under a strong magnetic field. Pirmohammadi and Ghassemi (2009) numerically studied the effect of a magnetic field on natural convection heat transfer inside a tilted square enclosure. They found that for a given inclination angle, as the value of Hartmann number increases, the convective heat transfer reduces. Furthermore, they achieved that at $Ra=10^4$, value of Nusselt number depends strongly upon the inclination angle for relatively small values of Hartmann number. Moreover, they demonstrated that at $Ra = 10^5$, $\phi = 0^\circ$ and $Ha = 70$ isotherms are vertical and therefore the main heat transfer mechanism is conduction. Sathiyamoorthy and Chamkha (2010) used different thermal boundary conditions to examine the steady laminar two-dimensional natural convection in the

presence of inclined magnetic field in a square enclosure filled with a liquid gallium. They have concluded that the heat transfer decreases with an increase of the magnetic field and that the vertically and horizontally applied magnetic fields influence the heat transfer differently.

Most of the studies on the natural convection in cavities with the magnetic effects have considered the electrically conducting fluid with a low thermal conductivity. This, in turn, limits the enhancement of heat transfer in the cavity particularly in the presence of the magnetic field. Nanofluids with enhanced thermal characteristics have widely been examined to improve the heat transfer performance of many engineering applications (Hosseini *et al.*, 2014, Ahmed and Eslamian, 2015). Khanafer *et al.* (2003) numerically investigated the heat transfer enhancement in a two-dimensional cavity utilizing nanofluids for various pertinent parameters. They tested different models for nanofluid density, viscosity, and thermal expansion coefficients. It was found that the suspended nanoparticles substantially increase the heat transfer rate at any given Grashof numbers. Natural convection heat transfer of nanofluids in a square cavity, heated isothermally from the vertical sides, has been studied numerically by Ho *et al.* (2008). They investigated the effect of various formulas for the effective thermal conductivity and dynamic viscosity of Al_2O_3 -water nanofluid on the heat transfer characteristics and showed that the uncertainties associated with different models adopted to model the nanofluids have a great effect on the natural convection heat transfer characteristics in the cavity. Santra *et al.* (2008) showed that heat transfer decline with increase of copper volume fraction in water for any Rayleigh numbers. Ghasemi *et al.* (2011) attempted magnetic field effect on natural convection in a nanofluid-filled square cavity. They have concluded that the heat transfer rate increases with an increase of the Rayleigh number but it decreases with an increase of the Hartmann number. Also exhibited that increase of the solid volume fraction may result in enhancement or deterioration of the heat transfer performance depending on the value of Hartmann and Rayleigh numbers.

The lattice Boltzmann method (LBM) is a powerful numerical technique based on kinetic theory for simulating fluid flows and modeling the physics in fluids and nanofluids (Succi, 2001; Yu *et al.*, 2003; Karimipour *et al.*, 2015). In comparison with the conventional CFD methods, the advantages of LBM include simple calculation procedure, simple and efficient implementation for parallel computation, easy and strong handling of complex geometries, and others. Kefayati *et al.* (2011) studied the effect of SiO_2 -water nanofluid for heat transfer improvement in tall enclosures by lattice Boltzmann method. They obtained that the average Nusselt number increases with volume fraction for the whole range of Rayleigh numbers and the aspect ratios. They also showed that the effect of nanoparticles on heat transfer enhances as the enclosure aspect ratio increases. Magnetic field effect on natural convection heat transfer in an

inclined L-shape cavity filled with nanofluid was studied by Sheikholeslami *et al.* (2013). They found that enhancement in heat transfer has reverse relationship with Hartmann number and Rayleigh number.

Four kinds of thermal lattice Boltzmann equation models have been implemented: the passive scalar approach, the multispeed approach (MS), the hybrid approach, and the double population distribution function (DDF) approach. Most works based on the DDF approach to model convective flows utilizes the Lattice Boltzmann Bhatnagar-Gross-Krook (LBGK) method, which is approximated by a relaxation process with a single relaxation time (SRT). Because of its extreme simplicity, the LBGK method has become the most popular lattice Boltzmann model in spite of its well-known deficiencies. However, this simplicity comes at the expense of numerical instability (Lallemand and Luo, 2000) and inaccuracy in implementing boundary conditions (Ginzburg and D’Humières, 2003), at least with regards the multispeed approach (He *et al.*, 1998; D’Orazio *et al.*, 2003). These deficiencies in the BGK models can be easily addressed by using the multiple relaxation-time models introduced by D’Humières (1992). Because of their advantages compared to the BGK method, the multi-relaxation-time lattice Boltzmann (MRT-LB) models have been successfully applied to a variety of isothermal and non-isothermal flows (Du *et al.*, 2006; Niu *et al.*, 2006; Zheng *et al.*, 2008; Rahmati *et al.*, 2009).

Thus, the present study aims at presenting a novel passive scalar approach leaning on the multi-relaxation-time lattice Boltzmann method (MRT-LBM) with D2Q9 lattice model for solving the flow field and the MRT-LBM with D2Q5 lattice model for temperature field to simulate the natural convection of TiO₂-water nanofluid in a square cavity under different directions of magnetic field. The results of 2-MRT-LBM are validated with previous numerical investigations and effects of all parameters (Rayleigh number, volume fraction, Hartmann number and magnetic field angle) on flow field and temperature distribution are also considered.

2. GOVERNING EQUATIONS

2.1. D2Q9-MRT-LBM Model for Simulation of Flow Field

For a MRT-LB model, a set of density distribution functions $\{f_i(\mathbf{x}, t)\}$ is defined on each lattice node \mathbf{x} . The collision step is executed in the moment space \mathbb{M} while the streaming step is performed in the velocity space \mathbb{V} .

The equation which is used for solving the flow field is given by the following formula:

$$\begin{aligned} &|f_i(\mathbf{x} + \mathbf{c}_i \Delta t, t + \Delta t)\rangle - |f_i(\mathbf{x}, t)\rangle = \\ &-M^{-1}S[|m_i(\mathbf{x}, t)\rangle - |m_i^{eq}(\mathbf{x}, t)\rangle] + |\mathbf{F}_i(\mathbf{x}, t)\rangle, \end{aligned} \quad (1)$$

where $|m_i(\mathbf{x}, t)\rangle$ and $|m_i^{eq}(\mathbf{x}, t)\rangle$ are vectors of moments, $|m\rangle = (m_0, m_1, m_2, \dots, m_8)^T$. The superscript T denotes transpose vector. Also, the force term in eq. (1) is the external force term and is defined as follow:

$$\begin{aligned} \mathbf{F} &= F_x \mathbf{i} + F_y \mathbf{j}, \\ F_x &= 3\omega_i \rho (A((v \sin \phi \cos \phi) - (u \sin^2 \phi))), \end{aligned} \quad (2)$$

$$F_y = 3\omega_i \rho ((g \beta(T - T_m) + A((v \sin \phi \cos \phi) - (v \cos^2 \phi))),$$

where A is defined by:

$$A = \frac{Ha^2 \nu}{n^2}, \quad (3)$$

and Hartmann number is defined as $Ha = LB \sqrt{\sigma / \mu}$. In this definition σ is electrical conductivity, B is the magnitude of the magnetic field, n is the lattice number and \square is the direction of magnetic field.

The mapping between discrete velocity space and moment space is achieved by the transformation matrix M which maps the vector $|f_i(\mathbf{x}, t)\rangle$ to the vector $|m_i(\mathbf{x}, t)\rangle$:

$$|m\rangle = M |f\rangle \text{ and } |f\rangle = M^{-1} |m\rangle. \quad (4)$$

In the present work, we use the D2Q9 model (see Fig. 1), and the nine discrete velocities are given by:

$$\mathbf{c}_i = \begin{cases} (0, 0) & , i = 0 \\ (\cos[(i-1)\pi/2], \sin[(i-1)\pi/2])c & , i = 1-4, \\ \sqrt{2}(\cos[(2i-9)\pi/4], \sin[(2i-9)\pi/4])c & , i = 5-8 \end{cases} \quad (5)$$

where $c = \Delta x / \Delta t$ is the particle velocity and the lattice spacing Δx is set to equal 1, as is the time step Δt ($\Delta x = \Delta t = 1$).

The matrix M for D2Q9 lattice model is:

$$M = \begin{bmatrix} 1 & 1 & 1 & 1 & 1 & 1 & 1 & 1 & 1 \\ -4 & -1 & -1 & -1 & -1 & 2 & 2 & 2 & 2 \\ 4 & -2 & -2 & -2 & -2 & 1 & 1 & 1 & 1 \\ 0 & 1 & 0 & -1 & 0 & 1 & -1 & -1 & 1 \\ 0 & -2 & 0 & 2 & 0 & 1 & -1 & -1 & 1 \\ 0 & 0 & 1 & 0 & -1 & 1 & 1 & -1 & -1 \\ 0 & 0 & -2 & 0 & 2 & 1 & 1 & -1 & -1 \\ 0 & 1 & -1 & 1 & -1 & 0 & 0 & 0 & 0 \\ 0 & 0 & 0 & 0 & 0 & 1 & -1 & 1 & -1 \end{bmatrix}, \quad (6)$$

the row vectors of M are mutually orthogonal, i.e., MM^T is a diagonal matrix non-normalized. This allows to easily computing M^{-1} according to:

$$M^{-1} = M^T (MM^T)^{-1}. \quad (7)$$

The nine moments for the D2Q9 model are:

$$|m\rangle = (\rho, e, \varepsilon, j_x, q_x, j_y, q_y, p_{xx}, p_{yy})^T, \quad (8)$$

where $m_0 = \rho$ is the fluid density, $m_1 = e$ is related

to the energy, $m_2 = \varepsilon$ is related to the energy square, $m_{3,5} = j_{x,y}$ are components of the momentum $(j_x, j_y) = (\rho u, \rho v)$, $m_{4,6} = q_{x,y}$ are related to components of the energy flux and $m_{7,8} = p_{xx,yy}$ are related to the components of the symmetric and traceless strain rate tensor.

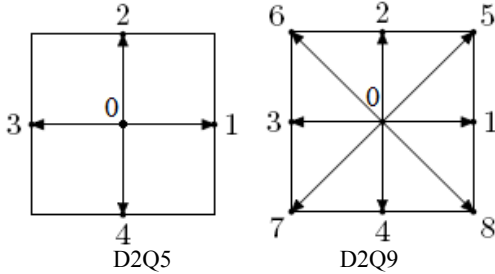


Fig. 1. D2Q5 and D2Q9 models.

The nine equilibrium moments of D2Q9 model are:

$$\begin{aligned} m_1^{eq} &= e^{eq} = -2\rho + 3(j_x^2 + j_y^2), \\ m_2^{eq} &= \varepsilon^{eq} = \rho - 3(j_x^2 + j_y^2), \\ m_4^{eq} &= q_x^{eq} = -j_x, \\ m_6^{eq} &= q_y^{eq} = -j_y, \\ m_7^{eq} &= p_{xx}^{eq} = (j_x^2 - j_y^2), \\ m_8^{eq} &= p_{xy}^{eq} = j_x j_y. \end{aligned} \tag{9}$$

with the above equilibrium moments, the sound speed of the lattice is $c_s = 1/\sqrt{3}$.

The diagonal matrix S is given by:

$$S = \text{diag}(1.0, 1.4, 1.4, s_3, 1.2, s_5, 1.2, s_7, s_8), \tag{10}$$

where $s_i \in (0, 2)$ for the non-conserved moments.

The choice of the relaxation parameters s_i can be determined by a linear stability analysis (Lallemand and Luo, 2000). s_3 and s_5 are arbitrary and can be set to unity. s_7, s_8 are chosen as the following:

$$s_7 = s_8 = 2 / (1 + 6\nu), \tag{11}$$

which ν is the kinematic viscosity of the fluid.

It should be mentioned here it is possible to recover the SRT-LBM by setting $s_1 = s_2 = s_4 = s_6 = s_7 = s_8 = 1/\tau$.

2.2 D2Q5-MRT-LBM Model for Simulation of Temperature Field

The energy conservation is modeled by an evolution equation. The distribution functions, noted \mathbf{g} , obey to the following equation:

$$\begin{aligned} |g_i(\mathbf{x} + \mathbf{c}_i \Delta t, t + \Delta t)\rangle - |g_i(\mathbf{x}, t)\rangle = \\ -\Omega \left[|g_i(\mathbf{x}, t)\rangle - |g_i^{eq}(\mathbf{x}, t)\rangle \right], \end{aligned} \tag{12}$$

For the D2Q5 model (Fig. 1.), the corresponding

lattice has five discrete velocities, and reads:

$$\mathbf{c}_i = \begin{cases} (0, 0) & , i = 0 \\ (\cos[(i-1)\pi/2], \sin[(i-1)\pi/2])c & , i = 0-4 \end{cases} \tag{13}$$

Ω represents the collision operator $\Omega = M^{-1}SM$, and the transformation matrix is given by:

$$M = \begin{bmatrix} 1 & 1 & 1 & 1 & 1 \\ 0 & 1 & 0 & -1 & 0 \\ 0 & 0 & 1 & 0 & -1 \\ -4 & 1 & 1 & 1 & 1 \\ 0 & 1 & -1 & 1 & -1 \end{bmatrix}, \tag{14}$$

Matrix M is invertible and orthogonal. The temperature T is the only conserved quantity and can be computed by:

$$T = \sum_{i=0}^4 g_i. \tag{15}$$

The equilibrium moments, m^{eq} corresponding to the distribution functions \mathbf{g} , can be written as:

$$m_0^{eq} = T, \quad m_1^{eq} = uT, \quad m_2^{eq} = vT, \quad m_3^{eq} = aT, \quad m_4^{eq} = 0, \tag{16}$$

Which a is a constant. The diagonal relaxation matrix S is given by:

$$S = \text{diag}(1, s_1, s_2, s_3, s_4), \tag{17}$$

The choice of s_i is discussed in details in Wang *et al.*, (2013). In this work, s_i is chosen as the following:

$$\begin{aligned} \frac{1}{s_1} - \frac{1}{2} = \frac{1}{s_2} - \frac{1}{2} = \frac{\sqrt{3}}{6}, \\ \frac{1}{s_3} - \frac{1}{2} = \frac{1}{s_4} - \frac{1}{2} = \frac{1}{6}, \end{aligned} \tag{18}$$

The above parameters lead to the thermal diffusivity:

$$\alpha = \frac{\sqrt{3}(4+a)}{60}, \tag{19}$$

where the constant a must be maintained $a < 1$ in order to avoid numerical instability of the D2Q5 model (Ginzburg *et al.*, 2010; Wang *et al.*, 2013).

The corresponding form of the equilibrium for the distribution functions \mathbf{g} is given by:

$$g_i^{eq} = \omega_i T (1 + 3\mathbf{c}_i \cdot \mathbf{u}), \tag{20}$$

where $\omega_0 = 0$ and $\omega_{1-4} = 1/4$ are D2Q5 lattice constants.

2.3. The Classic Equations for MHD Natural Convection

The incompressible Navier-stokes equations can be derived from this method using a Chapman-Enskog multi-scale expansion. More details are presented in Du *et al.* (2006). From this expansion, the continuity equation, the momentum equations

and the energy equations for MHD natural convection are written as:

$$\frac{\partial u}{\partial x} + \frac{\partial v}{\partial y} = 0. \quad (21)$$

$$\rho \left(u \frac{\partial u}{\partial x} + v \frac{\partial u}{\partial y} \right) = -\frac{\partial p}{\partial x} + \mu \left(\frac{\partial^2 u}{\partial x^2} + \frac{\partial^2 u}{\partial y^2} \right) + F_x. \quad (22)$$

$$\rho \left(u \frac{\partial v}{\partial x} + v \frac{\partial v}{\partial y} \right) = -\frac{\partial p}{\partial y} + \mu \left(\frac{\partial^2 v}{\partial x^2} + \frac{\partial^2 v}{\partial y^2} \right) + F_y. \quad (23)$$

$$u \frac{\partial T}{\partial x} + v \frac{\partial T}{\partial y} = \alpha \left(\frac{\partial^2 T}{\partial x^2} + \frac{\partial^2 T}{\partial y^2} \right). \quad (24)$$

In the above equations F_x and F_y are the total body forces in x and y directions, respectively, and they are defined as follows:

$$F_x = \frac{Ha^2 \mu}{L^2} (v \sin \phi \cos \phi - u \sin^2 \phi), \quad (25)$$

$$F_y = \rho g \beta (T - T_m) + \frac{Ha^2 \mu}{L^2} (u \sin \phi \cos \phi - v \cos^2 \phi). \quad (26)$$

2.4. Boundary Conditions

2.4.1. Boundary Conditions for Flow Field

Bounce-back boundary conditions are applied on all solid boundaries, which mean that incoming boundary populations are equal to out-going populations after the collision. So, the following conditions are imposed:

For the north boundary:

$$f_4 = f_2, \quad f_7 = f_5, \quad f_8 = f_6. \quad (27)$$

For the south boundary:

$$f_2 = f_4, \quad f_6 = f_8, \quad f_5 = f_7. \quad (28)$$

For the east boundary:

$$f_3 = f_1, \quad f_6 = f_8, \quad f_7 = f_5. \quad (29)$$

For the west boundary:

$$f_1 = f_3, \quad f_5 = f_7, \quad f_8 = f_6. \quad (30)$$

2.4.2. Boundary Conditions for Temperature Field

The adiabatic boundary condition is used on the north and south of the boundaries. For the north boundary, the following conditions are imposed:

$$g_{i,n} = g_{i,n-1}, \quad i = 0, \dots, 4. \quad (31)$$

For the south boundary:

$$g_{i,0} = g_{i,1}, \quad i = 0, \dots, 4. \quad (32)$$

In addition, for the east and west boundaries the following conditions are used (Wang *et al.*, 2013):

For the east boundary:

$$g_3 = -g_1. \quad (33)$$

For the west boundary:

$$g_1 = -g_3 + 2\sqrt{3}\alpha T_h. \quad (34)$$

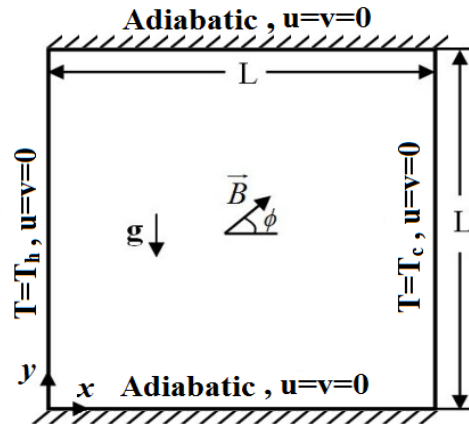


Fig. 2. Geometry and boundary conditions of the present study.

3. DESCRIPTION OF PROBLEM

3.1. The Geometry Description

The geometry of the present problem is shown in Fig. 2. It consists of a two-dimensional square cavity with the height of L . The cavity is bounded by two isothermal vertical walls at temperatures T_h and T_c and by two horizontal adiabatic walls. The horizontal walls are assumed to be insulated, non conducting, and impermeable to mass transfer. The cavity is filled with a mixture of water and solid TiO_2 . The nanofluid in the cavity is Newtonian, incompressible, and laminar. Thermo-physical properties of the base fluid and the nanoparticles are given in Table 1. A uniform magnetic field (\mathbf{B}) with a constant magnitude B is applied at inclined angle ϕ from the horizontal plane. It is assumed that the induced magnetic field produced by the motion of an electrically conducting fluid is negligible compared to the applied magnetic field. Furthermore, it is assumed that the viscous dissipation and Joule heating are neglected.

Table 1 Thermo-physical properties of water and nanoparticles (Abu-Nada *et al.*, 2008)

	Pr	ρ (kg/m ³)	C_p (J/kg K)	k (W/m K)	β (K ⁻¹)	μ (W/m K)
Water	6.2	997.1	4179	0.613	21×10^{-5}	0.001003
TiO ₂	-	4250	686.2	8.9538	0.9×10^{-5}	-

3.2. Method of Natural Convection Solution

To ensure that the code works in near incompressible regime, the characteristic velocity ($U_0 = \sqrt{g\beta\Delta TL}$) regime must be small compared

with the fluid speed of sound. In this work, the characteristic velocity selected is 0.1 of sound speed. By fixing Rayleigh number, Prandtl number and Mach number, the viscosity and thermal diffusivity are calculated from definition of these.

$$\nu = \sqrt{\frac{Ma^2 n^2 Pr c_s^2}{Ra}} \quad (35)$$

Rayleigh and Prandtl numbers are defined as:

$$Ra = \frac{g \beta L^3 Pr (T_h - T_c)}{\nu^2}, \quad Pr = \frac{\nu}{\alpha} \quad (36)$$

Furthermore speed of sound is constant ($c_s = 1/\sqrt{3}$). Finally, the values of relaxation times for flow and temperature can be found by the obtained viscosity and thermal diffusivity.

3.3. The Lattice Boltzmann Model for Nanofluid

The thermo-physical properties of the nanofluid are assumed to be constant (Table 1) except for the density variation, which is approximated by the Boussinesq approximation. The effect of density at reference temperature is given by (Cheng, 2011):

$$\rho_{nf} = (1 - \phi)\rho_f + \phi\rho_s, \quad (37)$$

whereas the heat capacitance of the nanofluid is (Cheng, 2011):

$$(\rho C_p)_{nf} = (1 - \phi)(\rho C_p)_f + \phi(\rho C_p)_s, \quad (38)$$

With ϕ being the volume fraction of the solid particles. The viscosity of the nanofluid containing a dilute suspension of small rigid spherical particles is given by Brinkman model (Khanafar *et al.*, 2003) as:

$$\mu_{nf} = \frac{\mu_f}{(1 - \phi)^{2.5}} \quad (39)$$

The effective thermal conductivity of the nanofluid can be approximated by the Maxwell-Garnett model where the nanoparticles is assumed to be the same and have spherical shapes (Khanafar *et al.*, 2003):

$$\frac{k_{nf}}{k_f} = \frac{k_s + 2k_f + 2\phi(k_f - k_s)}{k_s + 2k_f - \phi(k_f - k_s)} \quad (40)$$

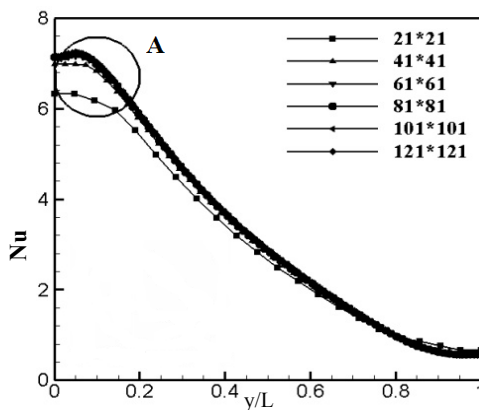


Fig. 3. Local Nusselt number on the hot wall for different uniform grids.

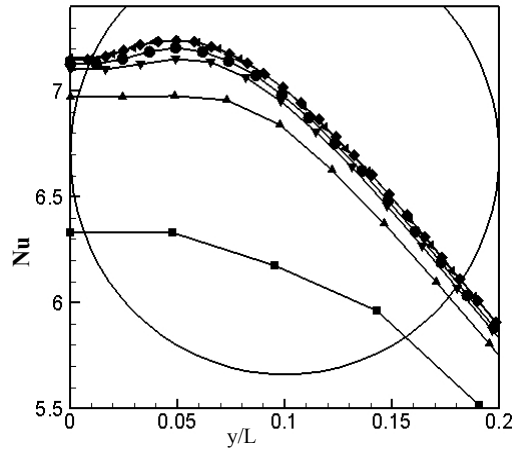


Fig. 4. Enlarged region A in fig. 3.

Nusselt number is one of the most important dimensionless parameters in describing the convective heat transfer. The local Nusselt number and the average value at the hot and cold walls are calculated as:

$$Nu = -\frac{k_{nf}}{k_f} \frac{L}{\Delta T} \frac{\partial T}{\partial x}, \quad (41)$$

$$Nu_{avg} = \frac{1}{L} \int_0^L Nu dy. \quad (42)$$

ΔT is the temperature difference between the hot and cold walls.

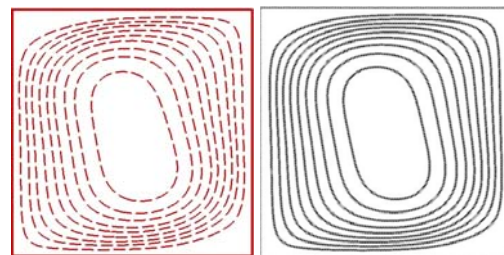


Fig. 5. Comparison of the Streamlines Between Numerical Results by Pirmohammadi and Ghasemi (2009) (—) and the present results (---) at $Ra = 10^5$, $Ha = 70$ and $\theta = 45^\circ$.

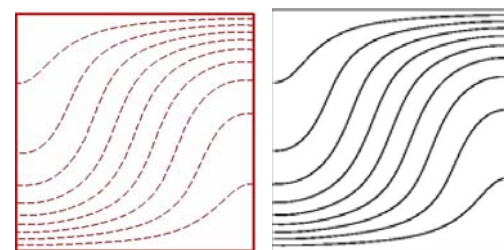


Fig. 6. Comparison of the isotherms between numerical results by Pirmohammadi and Ghasemi (2009) (—) by Pirmohammadi and Ghasemi (2009) (—) and the present results (---) at $Ra = 10^5$, $Ha = 50$ and $\theta = 90^\circ$.

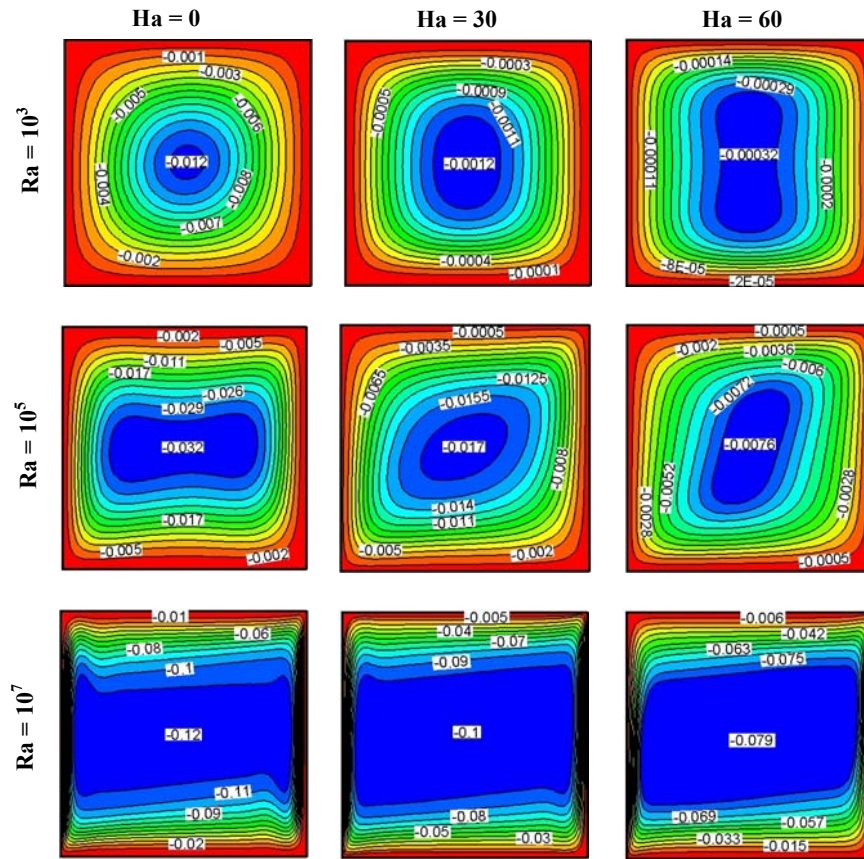


Fig. 7. Streamlines for different Rayleigh and Hartmann numbers ($\square = 0^\circ$ and $\phi = 3\%$).

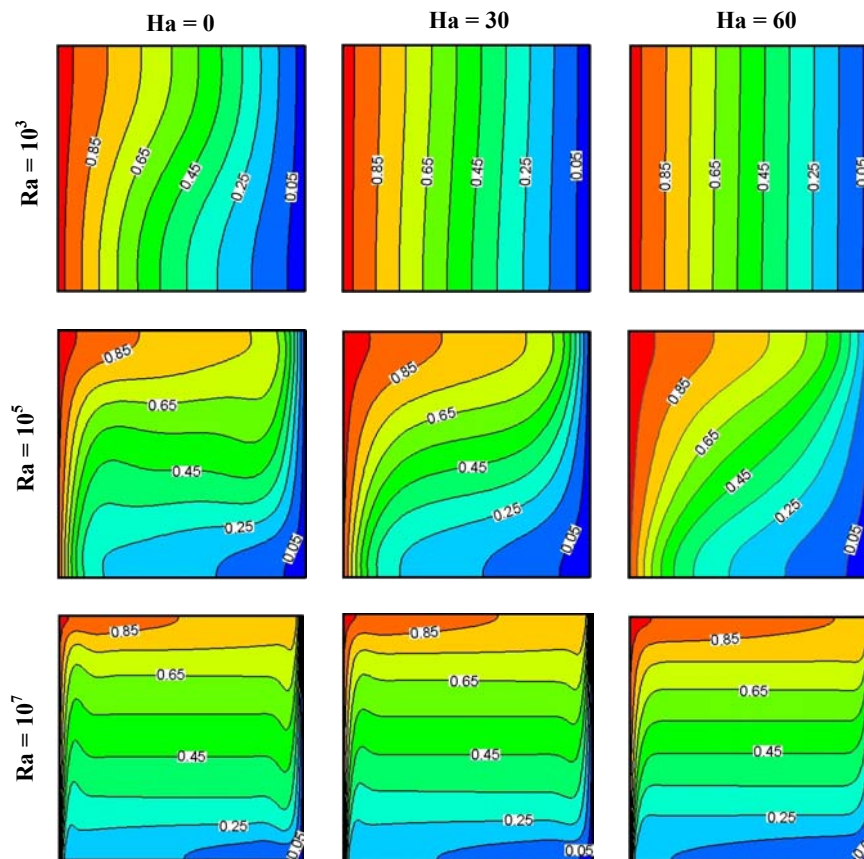


Fig. 8. Isotherms for different Rayleigh and Hartmann numbers ($\square = 0^\circ$ and $\phi = 3\%$).

Table 2 The averaged Nusselt number on the hot wall in comparison with Ghasemi *et al.* (2011)

Ra no.		$\phi = 0\%$	$\phi = 2\%$	$\phi = 4\%$
10^3	Ghasemi <i>et al.</i> (2011)	1.002	1.079	1.121
	Present Study	1.028	1.079	1.131
10^5	Ghasemi <i>et al.</i> (2011)	3.150	3.138	3.124
	Present Study	3.147	3.201	3.274
10^7	Ghasemi <i>et al.</i> (2011)	16.929	17.197	17.449
	Present Study	16.722	17.033	17.249

Finally, the following criterion to check for the steady-state solution was used:

$$Error = Max |T^{n+1} - T^n| \leq 10^{-8}. \quad (43)$$

4. CODE VALIDATION AND GRID INDEPENDENCE

An extensive mesh testing procedure was conducted to guarantee a grid independent solution. Six different mesh combinations were explored for the case of $Ra = 10^5$, $\phi = 5\%$, $\square = 0^\circ$ and $Ha = 30$. The present code was tested for grid independence by calculating the local Nusselt number on the hot wall. It was found in Figs. 3 and 4 that a grid size of 101×101 ensures the grid independent solution for the present case.

To check the accuracy of the present results, the present code is validated with Results of Pirmohammadi and Ghasemi (2009) and Ghasemi *et al.* (2011). As shown in Figs. 5 and 6, the streamlines and the isotherms have a good agreement with Pirmohammadi and Ghasemi (2009) work. Also, Table 2 show the results of MHD natural convection flow in an enclosed cavity filled by water- Al_2O_3 nanofluid which have been obtained by Ghasemi *et al.* (2011). As shown in this table, the obtained results of this work have a good agreement with Ghasemi *et al.* (2009) results.

5. RESULTS AND DISCUSSION

5.1. Effect of Hartmann and Rayleigh Numbers

Figures 7 and 8 show the effect of Hartmann number for three values of the Rayleigh number ($Ra=10^3, 10^5$ and 10^7) and for horizontal magnetic field ($\phi = 0^\circ$) on the streamlines and isotherms, respectively. The cavity is filled with a water- TiO_2 nanofluid, which has a solid volume fraction of $\phi = 3\%$. The buoyancy-driven circulating flows within

the cavity are evident for all values of the Rayleigh and Hartmann numbers. The strength of these circulations increases as the Rayleigh number increases and decreases as the Hartmann number increases. The results furthermore show for a low Rayleigh number, conduction is the dominant mechanism for heat transfer compared to the convection mechanism. However, by increasing the Rayleigh number the buoyancy forces increases and overcomes the viscous forces and the heat transfer is dominated by convection. The isotherms are affected by variations in the Hartmann number. These effects are more noticeable at $Ra = 10^5$, where an increase in the Hartmann number results in the isotherms changing they go from horizontal to vertical. This is an indication of weaker convection flows at higher Hartmann numbers.

Figure 9 illustrates the influence of the Hartmann number on the y-component of velocity vector along the horizontal mid-span of the cavity at three values of the Rayleigh number ($Ra = 10^3, 10^5, 10^7$) and for a solid volume fraction of $\phi = 3\%$ and for horizontal magnetic field ($\phi = 0^\circ$). The maximum y-component of velocity vector increases when the Rayleigh number increases due to the strong buoyancy driven flows and it decreases when the Hartmann number increases due to the effect of magnetic field on the convective flows. The effect of Hartmann number on the y-component of velocity vector profile is more significant at $Ra = 10^5$, where the convective flow field is not very strong and can be influenced by the magnetic field.

Figure 10 shows the effect of the Hartmann number on the local Nusselt number along the hot wall of the cavity at three values of the Rayleigh number ($Ra = 10^3, 10^5, 10^7$) and for a solid volume fraction of $\phi = 3\%$. The simulation result shown in this figure indicates that due to the strengthened buoyant flow, the local Nusselt number increases as the Rayleigh number increases and due to the suppression of the convective circulating flows by the stronger magnetic field, it decreases as the Hartmann number increases. Changing the Hartmann number has a more noticeable effect on the local Nusselt number at $Ra = 10^5$, where the buoyant flows are significantly affected by the magnetic field. This finding is similar to that of the previous results.

Table 3 presents the effect of the Hartmann number on the average Nusselt number on the hot wall of the cavity at three values of Rayleigh number ($Ra = 10^3, 10^5, 10^7$) and for a solid volume fraction of $\phi = 3\%$ and for horizontal magnetic field ($\phi = 0^\circ$). It is observed that the effect of Hartmann number is opposite to the effect of Rayleigh number. For all values of the Hartmann numbers, the results show that average Nusselt number increase as the Rayleigh number increases. This is due to the increasing strength of the buoyancy-driven flow within the cavity as the as the Rayleigh number increases. For all values of the Rayleigh numbers, with an increasing in the Hartmann number, the average Nusselt number decreases. As pointed in the previous results, changing the Hartmann number has a more noticeable effect on the local Nusselt number at $Ra = 10^5$.

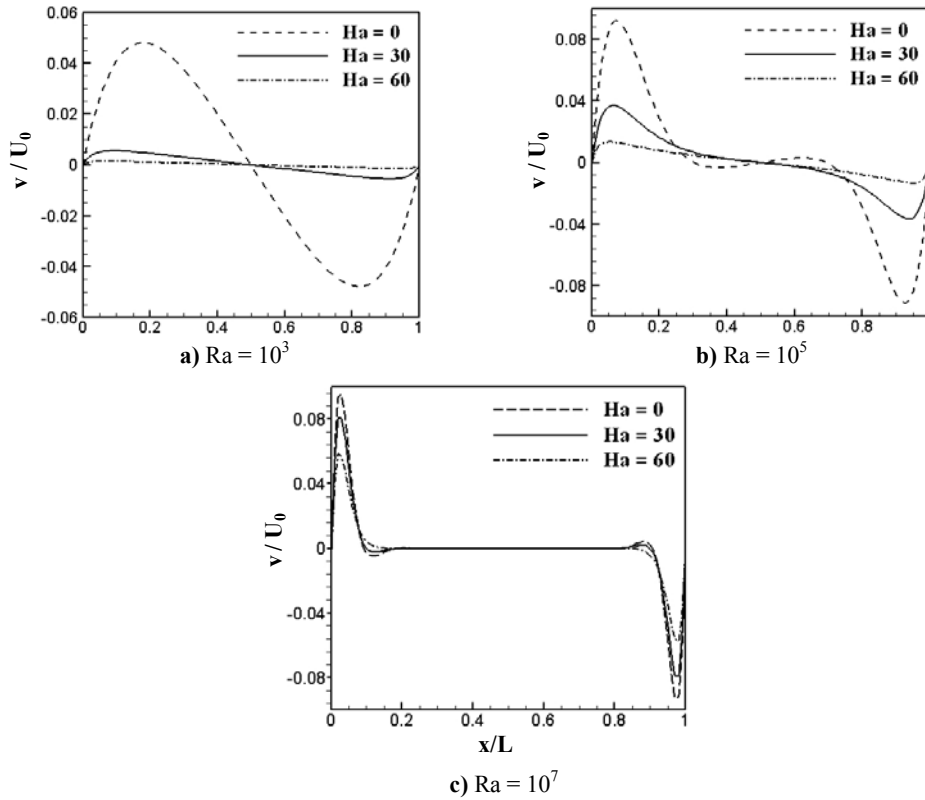


Fig. 9. Variation of y-component of velocity vector along the mid-span of the cavity for different Rayleigh numbers at $\phi = 3\%$ and $\theta = 0^\circ$.

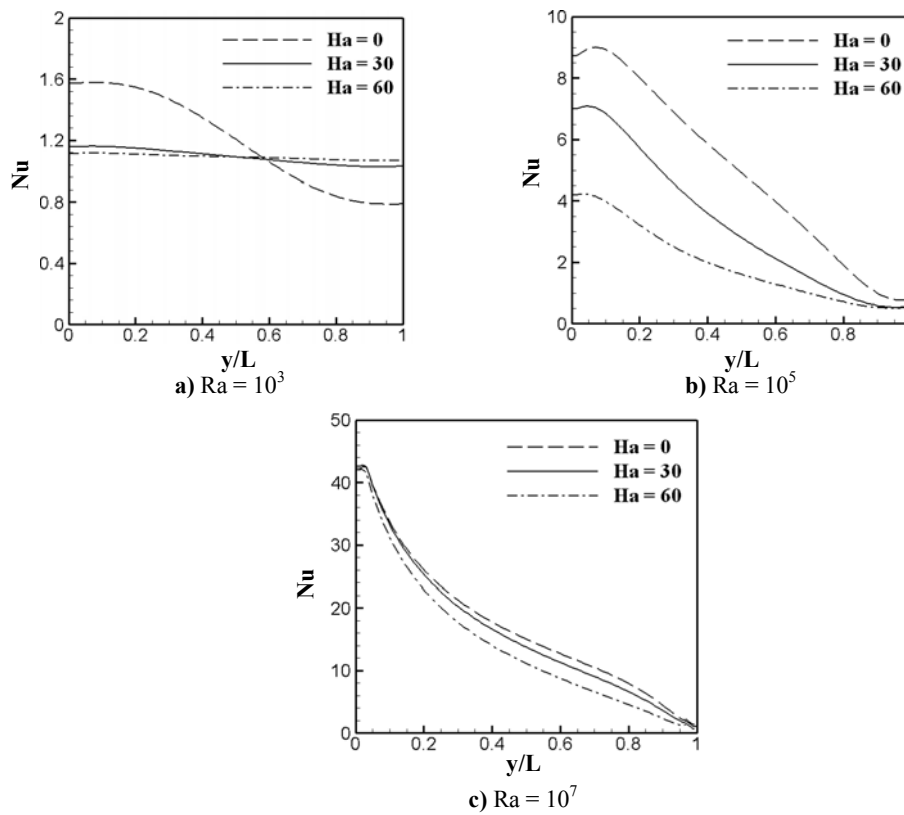


Fig. 10. Local Nusselt number along the hot wall of the cavity for different Rayleigh numbers at $\phi = 3\%$ and $\theta = 0^\circ$.

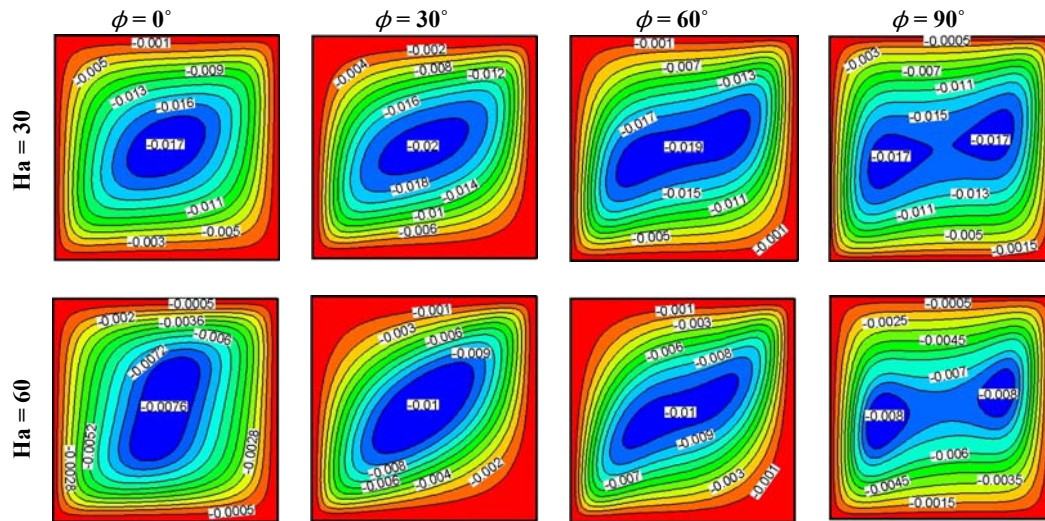


Fig. 11. Streamlines for different Hartmann number and ϕ for $\phi = 3\%$ and $Ra = 10^5$.

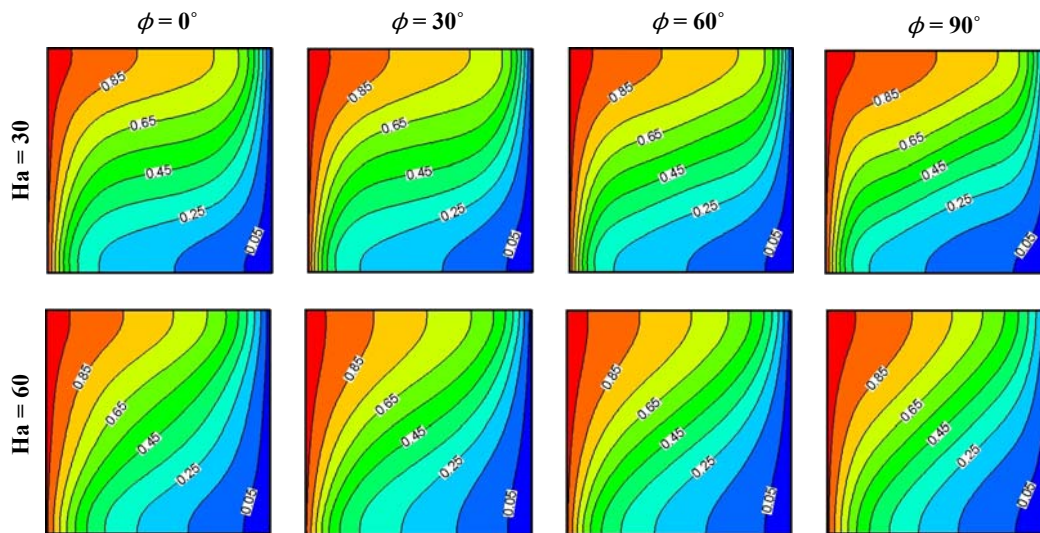


Fig. 12. Isotherms for different Hartmann number and ϕ for $\phi = 3\%$ and $Ra = 10^5$.

Table 3 Average Nusselt number at $\phi = 3\%$ and $\phi = 0^\circ$

	Ha = 0	Ha = 30	Ha = 60
Ra = 10^3	1.207	1.105	1.102
Ra = 10^5	4.975	3.287	1.944
Ra = 10^7	17.396	16.818	14.336

Table 4 Average Nusselt number for Ha = 30 and $\phi = 3\%$

Ra	$\phi = 0^\circ$	$\phi = 30^\circ$	$\phi = 60^\circ$	$\phi = 90^\circ$
10^3	1.104	1.104	1.104	1.104
10^7	16.434	16.661	16.982	17.133

5.2 Effect of the Magnetic Field Direction

The change of the magnetic field direction causes the modification of the Lorentz force direction relative to the gradient temperature which controls

the heat transfer rate.

Figures 11 and 12 illustrate the influence of the direction of the magnetic field on the streamline and isotherm contours on nanofluid ($\phi = 3\%$) for two values of the Hartmann number ($Ha = 30$ and 60) and for $Ra = 10^5$. The effect of magnetic field angle on isotherms is almost negligible. It can be seen that the effect of inclination angles on the flow is considerable significant with an increase of magnetic fields. For all Hartmann number two horizontal eddies occur when $\phi = 90^\circ$. With an increase in the Hartmann number and for $Ha = 60$ and when ϕ is zero, the Lorentz force only acts in the y-direction. Considering the symmetry, the x-component of velocity vector is dominant at the vertical centerline due to $v = 0$, which means the total speed is almost parallel to the magnetic field and therefore the magnetic force is close to zero. Because the magnetic force can reduce the effect of buoyancy, the total force at the vertical centerline is larger than that in the other areas. As the result, the conducting fluids are stretched more significant

near the vertical centerline. For all Hartmann number, with increasing in the magnetic field angle the Lorentz force reduce the x-component of velocity vector and the streamlines form the horizontal shape.

Figure 13 exhibits the variation of the profile of y-component of velocity vector along horizontal centerline ($y = 0.5$) with different angles. As explained in the previous, with an increasing in the magnetic field angle the magnetic field effect (Lorentz force) in the y-direction reduces and the y-component of velocity vector increase.

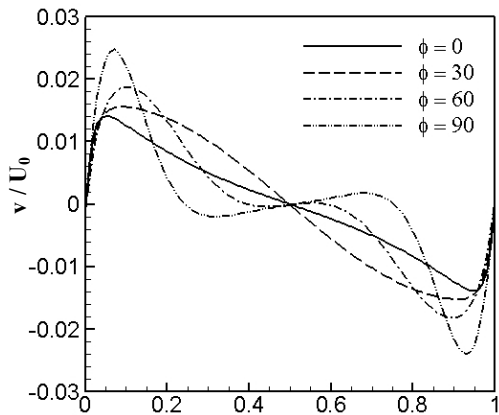


Fig. 13. Comparisons of v-velocity along the horizontal centerline for different magnetic field angles at $Ra = 10^5$ and $Ha = 60$ and $\phi = 3\%$.

Table 4 Average Nusselt number for $Ha = 30$ and $\phi = 3\%$.

Ra	$\phi = 0^\circ$	$\phi = 30^\circ$	$\phi = 60^\circ$	$\phi = 90^\circ$
10^3	1.104	1.104	1.104	1.104
10^7	16.434	16.661	16.982	17.133

Figure 14 shows the variation of local Nusselt number along the hot wall by varying the direction of magnetic field for $Ra = 10^5$, $Ha = 30$ and $\phi = 3\%$. With increasing the magnetic field angle from 0° to 60° , the local Nusselt number enhances. This mean that the Lorentz force decrease and so the local Nusselt number increases. With increasing the magnetic field angle from 60° to 90° the Lorentz force conquest the buoyancy force and the local Nusselt number decreases.

Figure 15 shows the variation of average Nusselt number along the hot wall by varying the direction of magnetic field for $Ra = 10^5$, $Ha = 30, 60$ and $\phi = 3\%$. For $Ha = 30$ with increasing the magnetic field angle to 60° the average Nusselt number increase but for $Ha = 60$ due to increasing the Lorentz force, the enhancement on the average Nusselt number is from magnetic angle of 0° to 30° and with increasing ϕ to 90° , the average Nusselt number decreases.

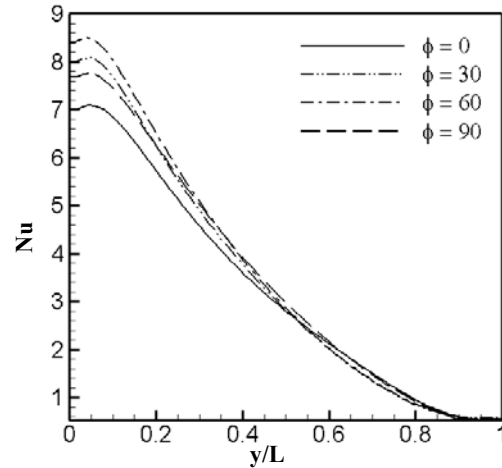


Fig. 14. Variation of the local Nusselt number on the hot wall for $Ra = 10^5$, $Ha = 30$ and $\phi = 3\%$ for different ϕ .

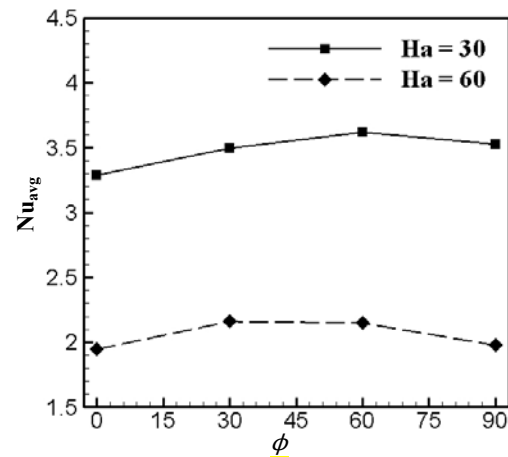


Fig. 15. Variation of the average Nusselt number for $Ra = 10^5$, $Ha = 30, 60$ and $\phi = 3\%$ for different ϕ .

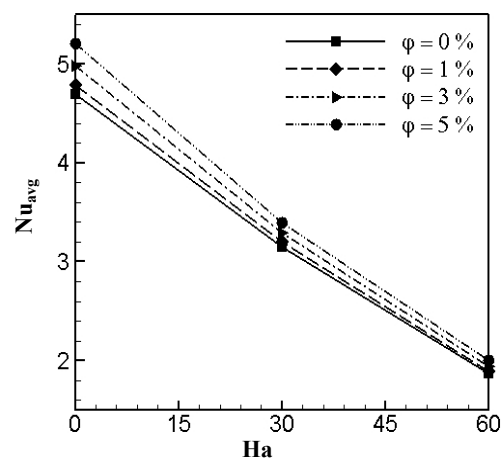


Fig. 16. Variation of the average Nusselt number with Hartmann number for different volume fraction and for $\phi = 0^\circ$ and $Ra = 10^5$.

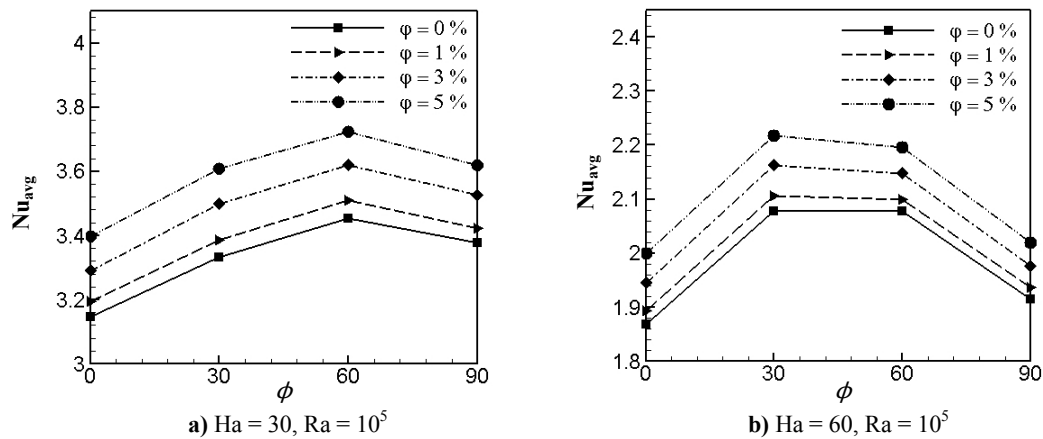


Fig. 17. Variation of the average Nusselt number with magnetic field angle for different volume fraction and different Hartmann number.

Table 4 presents the effects of magnetic field angle on the average Nusselt number on the hot wall of the cavity at two values of the Rayleigh number ($Ra = 10^3, 10^7$) and for a solid volume fraction of $\phi = 3\%$ and for $Ha = 30$. At low Rayleigh numbers ($Ra = 10^3$) the buoyancy-driven circulating flows is weak and the effect of magnetic field angle on the average Nusselt number is negligible. At high Rayleigh number ($Ra = 10^7$) with an increase in the magnetic field angle the effect of magnetic field decreases and the average Nusselt number increase.

5.3. Effect of Solid Volume Fraction

Figure 16 illustrates the influence of the Hartmann number and solid volume fraction on the average Nusselt number at $Ra = 10^5$ and $\phi = 0^\circ$. As shown in this figure, for all Hartmann number the average Nusselt number increases as solid volume fraction increases. It is obvious that the effect of the solid volume fraction on average Nusselt number declines with the enhancement of Hartmann number.

Figures 17.a and 17.b present the influence of the direction of the magnetic field and solid volume fraction on the average Nusselt number at $Ra = 10^5$ and for several Hartmann number. As shown in this figures, for all Hartmann number, adding nanoparticles augments the average Nusselt number at the hot wall of the cavity. The magnetic field influence on the effect of nanoparticles on the average Nusselt number enhancement is not significant.

6. CONCLUSION

In this work, a double multi-relaxation-time lattice Boltzmann method is proposed to simulate MHD natural convection of TiO_2 -water nanofluid in a two-dimensional square cavity. The key point in this proposed model is the use of two sets of distribution functions. A MRT-D2Q9 and MRT-D2Q5 lattice model are used to simulate the flow field and temperature field, respectively.

In order to validate the proposed model, the obtained results of this work have been compared

with previous numerical investigations. It was shown that the results predicted by the 2-MRT-LB method are in good agreement with other numerical results.

The obtained numerical results show that the 2-MRT-LB model is a powerful approach for simulating the MHD natural convection nanofluids in a two-dimensional square cavity and is able to study the effects of all parameter on the flow field and temperature field such as Rayleigh number, Hartmann number, magnetic field angle and solid volume fraction.

Stronger flow circulations within the cavity and intensified isotherms near the vertical walls are evident at higher Rayleigh numbers and at lower Hartmann numbers for a fixed solid volume fraction.

The y-velocity and temperature profiles along the horizontal mid-span of the cavity also show stronger flow fields within the cavity and higher temperature gradients near the vertical walls at higher Rayleigh numbers and lower Hartmann numbers.

The profiles of the local Nusselt number along the hot wall and the average Nusselt number verify that when the Hartmann number increases, the heat transfer rate decreases. The rate of this decrease is a function of the Rayleigh number. The most significant influence of the Hartmann number on the heat transfer deterioration occurs at $Ra = 10^5$, where the buoyancy-driven flow starts to dominate the heat transfer mechanism.

For all Hartmann numbers ($Ha = 30, 60$), with increasing in the magnetic field angle the Lorentz force reduce the u-velocity and the streamlines form the horizontal shape.

With an increasing in the magnetic field angle the magnetic field effect in the y-direction reduces and the v-velocity increases.

With increasing the magnetic field angle from 0° to 60° local Nusselt number enhances and with increasing the magnetic field angle from 60° to 90°

the Lorentz force conquest the buoyancy force and the local Nusselt number decreases.

By adding nanoparticles to fluid, the average Nusselt number increases, and by increasing the volume fraction, this phenomenon becomes more sensible. The magnetic field effect on the effect of nanoparticles on the heat transfer enhancement is not significant.

REFERENCES

- Abu-Nada, E., Z. Masoud and A. Hijazi (2008). Natural convection heat transfer enhancement in horizontal concentric annuli using nanofluids. *International Communications in Heat and Mass Transfer* 35, 657-665.
- Ahmed, M. and M. Eslamian (2015). Laminar forced convection of a nanofluid in a microchannel: Effect of flow inertia and external forces on heat transfer and fluid flow characteristics. *Applied Thermal Engineering* 78, 326-338.
- Aminossadati, S. M., A. Raisi and B. Ghasemi (2011). Effects of magnetic field on nanofluid forced convection in a partially heated microchannel. *International Journal of Non-Linear Mechanics* 46(10), 1373-1382.
- Cheng, T. S. (2011). Characteristics of mixed convection heat transfer in a lid-driven square cavity with various Richardson and Prandtl numbers. *International Journal of Thermal Sciences* 50, 197-205.
- D'Humieres, D. (1992). *Progress in Astronautics and Aeronautics*, AIAA, Washington, DC.
- D'Orazio, A., S. Succi and C. Arrighetti (2003). Lattice Boltzmann simulation of open flows with heat transfer. *Physics of Fluids* 15(9), 2778-2781.
- Du, R., B. Shi and X. Chen (2006). Multi-relaxation time lattice Boltzmann model for incompressible flow. *Physics Letters A* 359, 564-572.
- Garandet, J. P., J. P. Alboussiere and T. Moreau (1992). Buoyancy driven convection in a rectangular cavity with a transverse magnetic field. *International Journal of Heat and Mass Transfer* 35, 741-748.
- Ghasemi, B., S. M. Aminossadati and A. Raisi (2011). Magnetic field effect on natural convection in a nanofluid-filled square enclosure. *International Journal of Thermal Sciences* 50, 1748-1756.
- Ginzburg, I., D. D'Humieres and A. Kuzmin (2010). Optimal stability of advection diffusion lattice Boltzmann models with two relaxation times for positive/negative equilibrium. *Journal of Statistical Physics* 139(6), 1090-1143.
- Ginzburg, I. and D. D'Humieres (2003). Multi-reflection boundary conditions for lattice Boltzmann models. *Physical Review E* 68, 066614.
- He, X., S. Chen and G. D. Doolen (1998). A novel thermal model for the lattice Boltzmann method in incompressible limit. *Journal of Computational Physics* 146, 282-300.
- Ho, C. J., M. W. Chen and Z. W. Li (2008). Numerical simulation of natural convection of nanofluid in a square enclosure: effects due to uncertainties of viscosity and thermal conductivity. *International Journal of Heat and Mass Transfer* 51, 4506-4516.
- Hosseini, M., M. T. Mustafa, M. Jafaryar and E. Mohammadian (2014). Nanofluid in tilted cavity with partially heated walls. *Journal of Molecular Liquids* 199, 545-551.
- Karimipour, A., A. Hossein Nezhad, A. D'Orazio, M. Hemmat Esfe, M. R. Safaeid and E. Shirani (2015). Simulation of copper-water nanofluid in a microchannel in slip flow regime using the lattice Boltzmann method. *European Journal of Mechanics B/Fluids* 49, 89-99.
- Kefayati, G. H. R., S. F. Hosseinizadeh, M. Gorji and H. Sajjadi (2011). Lattice Boltzmann simulation of natural convection in tall enclosures using water/SiO₂ nanofluid. *International Communications in Heat and Mass Transfer* 38, 798-805.
- Khanafer, K., K. Vafai and M. Lightstone (2003). Buoyancy-driven heat transfer enhancement in a two dimensional enclosure utilizing nanofluids. *International Journal of Heat and Mass Transfer* 46, 3639-3653.
- Lallemand, P. and L. S. Luo (2000). Theory of the lattice Boltzmann method: dispersion, dissipation, isotropy, Galilean invariance, and stability. *Physical review E* 61(6), 6546-6562.
- Mahmoudi, A. H., I. Pop and M. Shahi (2012). Effect of magnetic field on natural convection in a triangular enclosure filled with nanofluid. *International Journal of Thermal Sciences* 59, 126-140.
- Niu, X. D., C. Shu, Y. T. Chew and Y. Peng (2006). A momentum exchange-based immersed boundary-lattice Boltzmann method for simulating incompressible viscous flows. *Physics Letters A* 354, 173-182.
- Okada, K. and H. Ozoe (1992). Experimental heat transfer rates of natural convection of molten gallium suppressed under an external magnetic field in either the X, Y, or Z direction. *Journal of Heat Transfer* 114, 107-114.
- Pirmohammadi, M. and M. Ghassemi (2009). Effect of magnetic field on convection heat transfer inside a tilted square enclosure. *International Communication in Heat and Mass Transfer* 36, 776-780.
- Rahmati, A. R., M. Ashrafizaadeh and E. Shirani (2009). Novel hybrid finite-difference thermal lattice Boltzmann models for convective flows. *Heat transfer research* 40(8).

- Rashidi, M. M., S. Abelman and N. Freidooni mehr (2013). Entropy generation in steady MHD flow due to a rotating porous disk in a nanofluid. *International Journal of Heat and Mass Transfer* 62, 515–525.
- Rudraiah, N., R. M. Barron, M. Venkatachalappa and C. K. Subbaraya (1995). Effect of a magnetic field on free convection in a rectangular enclosure. *International Journal of Engineering Science* 33, 1075-1084.
- Santra, A. K., S. Sen and N. Chakraborty (2008). Study of heat transfer augmentation in a differentially heated square cavity using copper–water nanofluid. *International Journal of Thermal Sciences* 47, 1113–1122.
- Sathiyamoorthy, M. and A. Chamkha (2010). Effect of magnetic field on natural convection flow in a liquid gallium filled square cavity for linearly heated side wall(s). *International Journal of Thermal Sciences* 49(9), 1856-1865.
- Sheikholeslami, M., M. Gorji-Bandpy and G. Domairry (2008). Free convection of nanofluid filled enclosure using lattice Boltzmann method (LBM). *Applied Mathematics and Mechanics (English Ed.)* 34(7), 1-15.
- Succi, S. (2001). *The Lattice Boltzmann Equation for Fluid Dynamics and Beyond*. Clarendon Press, Oxford.
- Utech, H. P. and M. C. Flemmings (1996). Elimination of solute banding in indium antimonite crystals by growth in a magnetic field. *Journal of Applied Physics* 37, 2021-2024.
- Vives, C. and C. Perry (1987). Effects of magnetically damped convection during the controlled solidification of metals and alloys. *International Journal of Heat Transfer* 30, 479-496.
- Wang, J., D. Wang, P. Lallemand and L. S. Luo (2013). Lattice Boltzmann simulation of thermal convective flows in two dimensions. *computational mathematics applications* 65, 262-286.
- Yu, D., R. Mei, L. S. Luo and W. Shyy (2003). Viscous flow computations with the method of lattice Boltzmann equation. *Progress in Aerospace Sciences* 39, 329-367.
- Zheng, L., B. Shi and Z. Guo (2008). Multiple-relaxation-time model for the correct thermo hydrodynamic equations. *Physical Review E* 78, 026705.